Chapter 4

The Influence of Ozone and Other Factors on Surface Radiation

4.1 Introduction

Ozone is important because of its interactions with solar radiation and with thermal radiation emitted by the atmosphere and the earth's surface. Partial absorption by ozone moderates the amount of solar UV radiation that reaches the ground. Increases in exposure to this radiation, particularly in the UV-B range, can be harmful to living organisms. Absorption by ozone and the influences of other variable factors on UV radiation are the main subjects of this chapter.

Ozone is the main source of radiative heating in the stratosphere through its absorption of solar radiation in the UV and the 550–650 nm range of wavelengths. Also, because ozone is a greenhouse gas like carbon dioxide and water vapour, the increases in tropospheric ozone that have occurred during this century have had a warming effect on the planet. On the other hand, the depletion of stratospheric ozone is likely to have partially offset the warming effects of increases in other greenhouse gases during the past two decades. These important roles of ozone are examined thoroughly in the WMO/UNEP and IPCC assessments [WMO 1991, 1994; IPCC 1990, 1994, 1995] but will not be addressed in detail here. In addition, ozone-depleting substances, notably the CFCs, are powerful greenhouse gases by virtue of their having absorption properties at wavelengths in the thermal infrared, where there is little absorption by other atmospheric constituents. These regions, between approximately 8 and 13 μm, are called the atmospheric infrared windows. Under various schemes of comparison it is estimated that CFC-11 and CFC-12 are from 2000 to 4000 times as effective as carbon dioxide as global warming agents. Ground-based measurements of the radiation emitted by several ozone-depleting gases are discussed in Section 4.3.

The effects of UV radiation on humans can be mitigated to some extent by changes in behaviour. The chapter therefore concludes with a discussion of two Canadian-developed programs, the Ozone Watch and the UV Index programs, that promote understanding of ozone depletion and the importance of reducing personal exposure to UV radiation.

4.1.1 Introduction to Ozone and UV Radiation.

Ozone absorbs so strongly in the UV-C range (below 280 nm) that solar radiation at these wavelengths does not reach the earth's surface. As the wavelength increases through the UV-B range (280–315 nm) and into the UV-A (315–400 nm), ozone absorption becomes weaker, until it is undetectable at about 340 nm. Figure 4.1 shows several spectra including the spectrum (A) of solar radiation measured above the atmosphere. The fractions of solar energy above the atmosphere in the UV-B and UV-A ranges are approximately 1.5% and 7% respectively. The figure also shows spectra measured at the ground near midday on two very clear days in mid-June. (These two spectra, curves B and C, are almost indistinguishable.) The fine curve (D) is computed from the extraterrestrial spectrum (A) and the absorption by the average measured ozone amount for the two days. It is above the measured ground-level spectra, but otherwise almost identical to them. One may conclude that, for these two clear days, the ground-level spectra are mostly the result of ozone absorption, with a relatively constant extra attenuation of about 40% due to air molecules and background aerosols.

The spectra in Figure 4.1 thus illustrate the simplest case in which ozone determines the intensity of solar UV radiation at ground level. In general, UV intensity varies considerably as a result of fluctations in cloud cover, ground albedo, aerosols, and other atmospheric constituents. In the context of possible

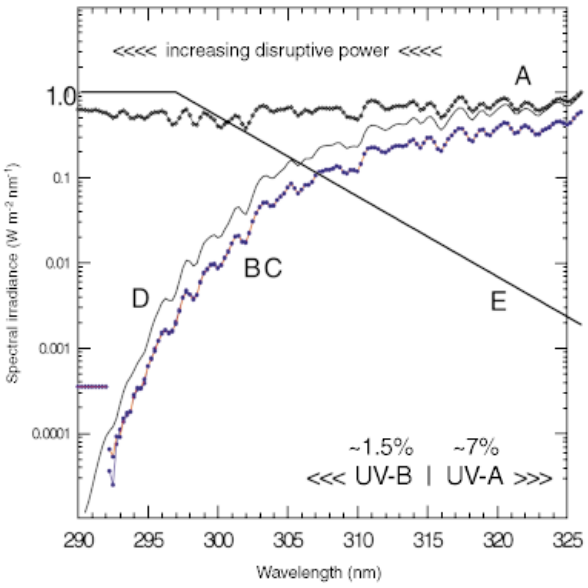

Figure 4.1 The solar spectrum above the atmosphere (A) and at ground level (B,C), ozone absorption (D), and sunburning (E).

biological consequences, the effect of an ozone-related change in the UV environment is likely to depend on how large that change is in comparison to the normal range of natural variability. For this reason, the variability and its causes must be studied more thoroughly.

Changes in UV radiation can be expressed in a variety of ways, and the question of which particular measure is most relevant to a given biological effect is often complex and difficult to resolve. One option is the total UV irradiation received over a specified area during the summer of each year. Over Toronto, for example, as shown later in this chapter, total summer irradiation at 300 nm has changed during the past decade by an amount comparable to the typical year-to-year variability and consistent with the observed ozone change. A statistical study based on satellite data [Lubin and Jensen 1995] reaches a similar conclusion for the change during the past 20 years in the erythemally weighted irradiation (i.e., weighted in terms of skin-reddening effectiveness) for July over southern Canada. Using monthly or seasonal irradiation as in these two examples is convenient but not necessarily correct in relation to a given biological effect, since some effects may be more dependent on peak values of UV encountered during the early growing season. However, statistics of peak values of UV or other derivative statistics have received little or no attention in the literature to date.

A similar question refers to what wavelengths should be considered. Action spectra, as discussed in Chapter 5, deal with the problem of impact variations across a range of wavelengths. An action spectrum, for a particular biological effect, expresses the effectiveness of radiation at each wavelength as a fraction of the effectiveness at a standard wavelength, such as 298 nm in the case of the erythemal action spectrum of the Commission internationale de l'éclairage (CIE). In principle, the wavelength integration of the product of an irradiance spectrum with the action spectrum yields the effectiveness of that spectrum at producing the given effect. For this to be valid, the effect must satisfy two requirements: first, additivity of effects at different wavelengths and, second, reciprocity, which means that the effect must depend on dose (irradiation) rather than dose rate (irradiance). Reciprocity and additivity are probably satisfied for a relatively simple effect like skin reddening, but there is no reason to expect them to be satisfied for other, more complex, effects. In this chapter, only the CIE action spectrum, curve E in Figure 4.1, has been illustrated. For a fairly wide range of atmospheric conditions, the CIE-weighted irradiance increases by approximately 1.2% for a decrease of 1.0% in the ozone value. The ratio 1.2 is called the radiometric amplification factor (RAF) of the CIE spectrum. Recently measured action spectra for plant damage [Quaite et al. 1992] and induction of squamous cell skin cancer in mice [deGruijl and van der Leun 1994] have RAFs that are also close to 1.2, while the full range of reported RAFs is from 0.2 to 4.0 [Madronich 1992].

4.2 Observed Dependencies of UV Changes on Ozone, Sulphur Dioxide, Clouds, Aerosol, and Snow

There is strong evidence to suggest that the total ozone decline in northern midlatitudes has been accompanied by increases in solar UV irradiance at the earth's surface [Kerr and McElroy 1993; Zerefos et al. 1995]. However, UV irradiance depends on many other variables, such as cloud condition, albedo, atmospheric aerosol, and pollution, that make it difficult to measure the effects of ozone decline on irradiance. Establishing a direct link between ozone and UV irradiance and separating the ozone-related component in UV irradiance from other components provides a better understanding of the causes of UV changes. The following are some of the approaches used to quantify that link.

Numerous studies [e.g., Frederick et al. 1993; Eck et al. 1995; Bojkov et al. 1995] show that it is possible to estimate UV irradiance from total ozone data. The reverse process, the derivation of total ozone amounts from UV radiation, is applied by the Dobson and Brewer methods when measuring total ozone using zenith sky radiance. However, to obtain reliable results it is necessary to have a set of parallel zenith sky and direct sun measurements [e.g., Komhyr 1980]. Stamnes et al. [1991] have also suggested the use of a radiative

transfer model to derive total ozone from measurements of horizontal irradiance at two wavelengths, 305 nm and 340 nm.

Total ozone may also be derived using the whole 290–325 nm irradiance spectrum measured by the Brewer spectrometer, and, conversely, the spectrum may be derived from the ozone amount [Fioletov et al. 1997]. A statistical model that relates the spectrum to the ozone amount and that was originally developed for quality control of UV spectral data is the basis of a new algorithm that is used to calculate the ozone value from the irradiance spectrum. This technique has proved to be a useful addition to the direct sun and zenith sky techniques.

UV irradiance measurements made by Brewer spectrophotometers at seven stations (Toronto, Edmonton, Winnipeg, Sapporo, Tateno, Kagoshima, and Naha) for the period 1989–1995 were used to establish the statistical model. The stations have between four and seven years of continuous UV observations and a set of parallel Dobson or Brewer total ozone measurements. All these data are available from the World Ozone and UV data Centre (WOUDC), Toronto.

There are two parts to the statistical analysis on which the model is based. The first is a comparison of irradiance values at all the wavelengths in the spectral range with the irradiance value at 324 nm, where ozone has least (and virtually negligible) absorption. This analysis primarily quantifies the dependence of UV-B irradiance on ozone. The second part of the analysis is the assessment of the absolute irradiance at 324 nm. Variation of irradiance at this wavelength is due to other causes besides ozone.

A discussion of observed dependencies of UV irradiance on ozone and other variables is given in the following sections.

4.2.1 Dependence on Ozone

Figure 4.2 shows the value of the mean logarithm of the ratio between solar irradiance at wavelength λ and irradiance at 324 nm as a function of wavelength and solar zenith angle for total ozone equal to 300 DU. For wavelengths between 305 and 315 nm the Umkehr effect [Götz 1931] is clearly seen: the ratio as a function of increasing zenith angle decreases up to a certain value of zenith angle and increases thereafter.

Comparison of the surface shown in Figure 4.2 with another surface representing a different total ozone value allows the calculation of the sensitivity of UV irradiance to changes in ozone as a function of wavelength and solar zenith angle. The sensitivities for a 1% decrease in ozone are shown in Figure 4.3.

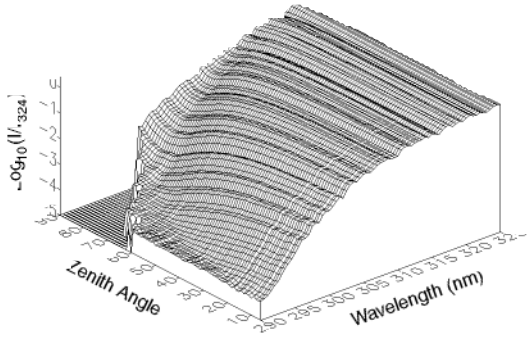

Figure 4.2 Logarithm of ratio between UV-B irradiance at wavelength λ and irradiance at 324 nm for 300 DU of total ozone as a function of zenith angle and wavelength.

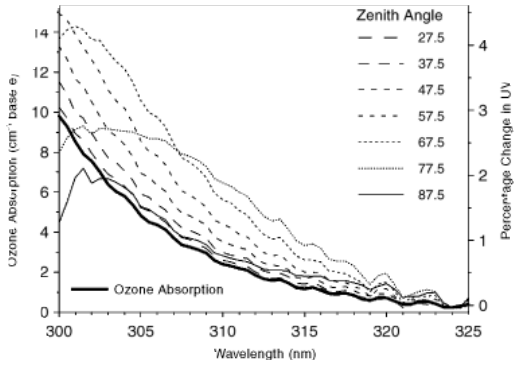

Figure 4.3 Sensitivity of UV irradiance to total ozone amount in percent change per 1% change in total ozone (for a total ozone amount of 300 DU) as a function of wavelength for different zenith angles. The bold continuous line shows the ozone absorption spectrum.

Figures 4.4a and 4.4b show measured and calculated spectra for two cases with approximately the same zenith angles and 324 nm irradiances but different total ozone values (about 250 and 500 DU respectively) and 3σ limits. The ratio of irradiance at any wavelength between 300 and 323 nm to that at 324 nm can be used to derive total ozone. Figures 4.4c and 4.4d show calculated total ozone as a function of wavelength. The accuracy of the retrieval depends on zenith angle and wavelength.

Total ozone was calculated from UV spectra which have been measured at Toronto since 1989. Figure 4.5 shows the monthly average departures from pre-1989 values for the UV spectral calculations compared with those of Brewer and Dobson direct sun measurements and satellite measurements. The agreement between all types of measurements is generally very good.

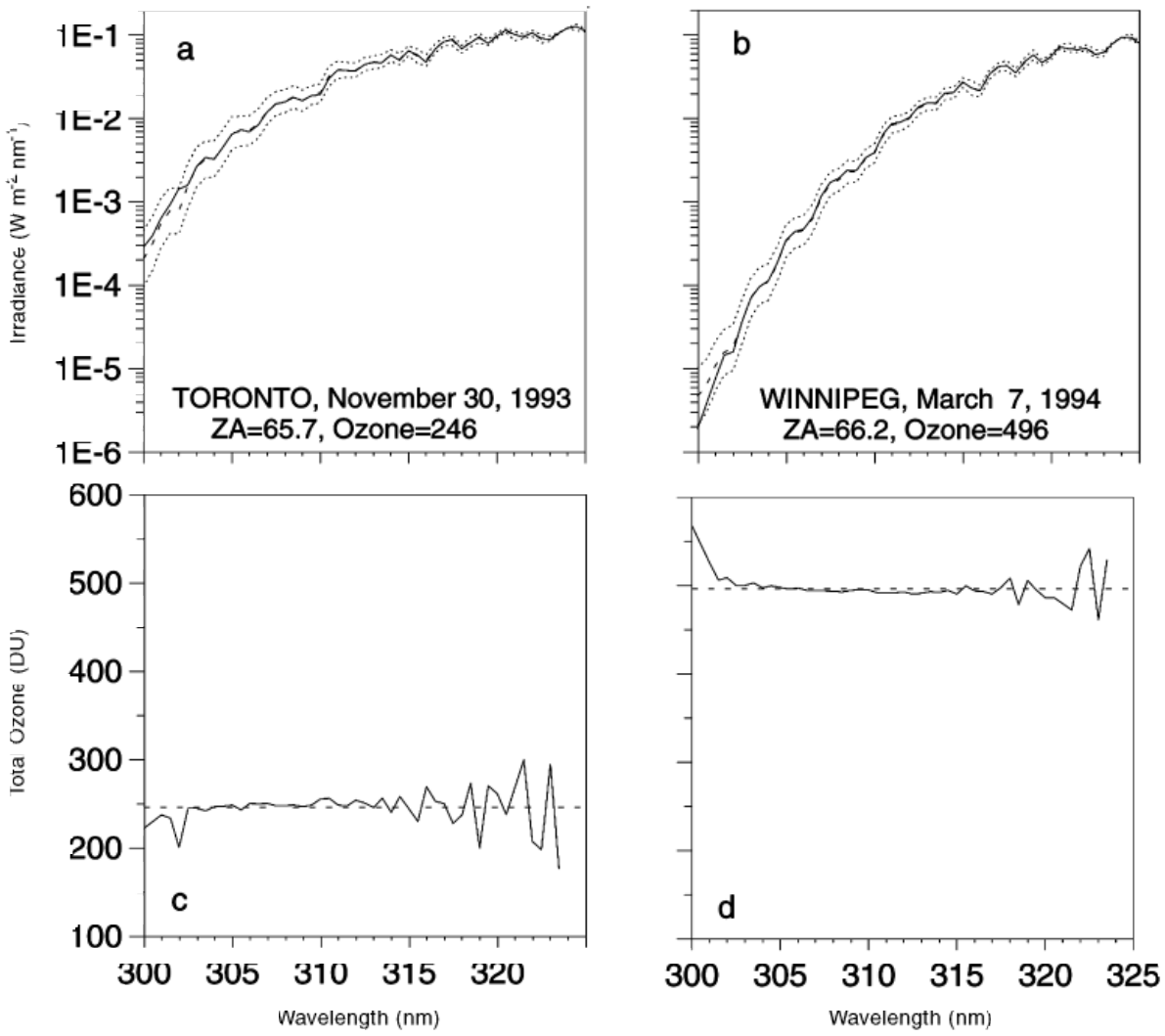

Figure 4.4 (a and b): Examples of two UV irradiance spectra (solid lines) measured for nearly the same zenith angles and 324 nm irradiance but for different total ozone amounts, estimated from Figure 4.2 (dashed lines) and the 3σ envelope (dotted lines). (c and d): Retrieved total ozone as a function of wavelength for the two spectra in (a) and (b), respectively. Dashed lines show direct sun total ozone measured values.

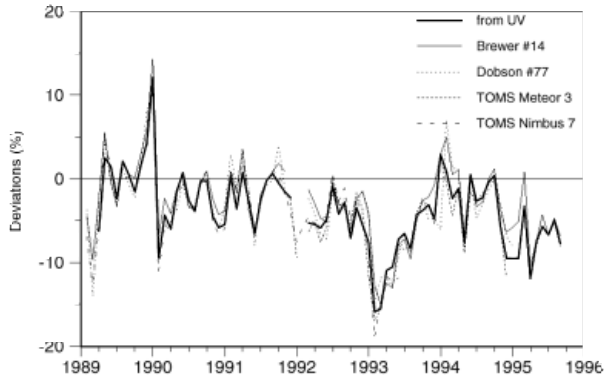

Figure 4.5 Monthly deviations of total ozone from pre-1989 level for Toronto, using Dobson #77 and Brewer #14 direct sun measurements, TOMS Nimbus 7 and Meteor 3 data, and retrieved estimates from Brewer #14 UV measurements.

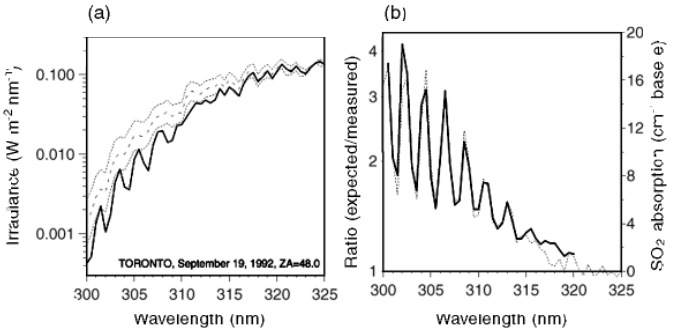

Figure 4.6 (a) Measured irradiance spectrum (solid line) and spectrum calculated from Figure 4.2 (dashed line) with 3σ envelope (dotted lines) for Toronto, September 19, 1992. (b) Ratio between estimated and measured irradiance (dotted line) and SO_2 absorption spectrum (solid line) of McGee and Burris [1987] at 210 K.

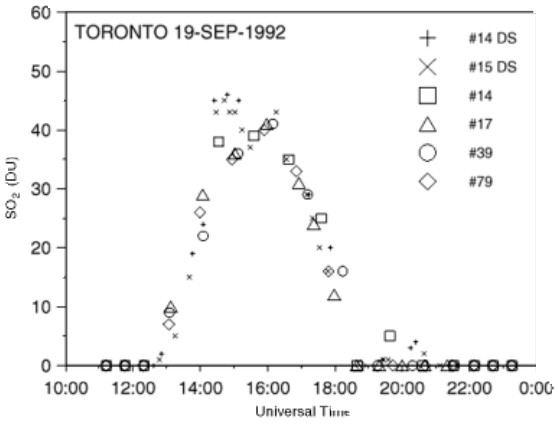

Figure 4.7 Total column sulphur dioxide derived from Brewer direct sun measurements (pluses and crosses) and from UV spectra (squares, triangles, circles, and diamonds) for September 19, 1992, at Toronto. Brewer instrument numbers are shown in the legend.

4.2.2 Dependence on SO_2

Occasionally, the measured UV spectrum will differ substantially from a spectrum predicted by the statistical model. One example is shown in Figure 4.6 (a) for Toronto on September 19, 1992, when the plume from the Mount Spurr, Alaska, volcanic eruption passed over the city [Krueger et al. 1995]. Most of the measured spectrum is outside the 3σ envelope and the difference exceeds 6σ at some wavelengths. The cause of these differences was identified as atmospheric SO_2, which has strong absorption bands in the UV-B spectral region, as shown in Figure 4.6 (b), for the resolution of the Brewer instrument. The ratio between the expected and measured spectra is also plotted. For some wavelengths the measured irradiance was 3 times lower than expected. The features of the ratio, however, reproduce the SO_2 absorption spectrum. Calculation of ozone from this spectrum results in values that overestimate ozone by 50 to 100 DU, depending on wavelength. The amount of SO_2 required to cause the absorption shown in Figure 4.6 is approximately 50 DU.

Figure 4.7 shows results of SO_2 values retrieved from UV spectra and direct sun SO_2 measurements for September 19, 1992, in Toronto. Both methods show the same pattern in SO_2 variations, and the difference between direct sun and global UV spectra methods is less than 20% for the time when maximum values of SO_2 were observed.

A summary of all days with more than 10 and 20 DU of SO_2 is shown for 13 localities in Table 4.1. Only days containing two or more observations at these levels have been included. The high SO_2 amounts over Kagoshima are associated with volcanic eruptions of nearby Mount Sakurajima and will be discussed further below. At all other stations, SO_2 levels above 20 DU were observed only once: that observation was recorded in Toronto when the plume from the Mount Spurr eruption passed overhead. Values between 10 and 20 DU were observed on fewer than 1% of the days, and most of these cases were associated with pollution. Since SO_2 values in the 10–20 DU range reduce the erythemally weighted UV irradiance by only a few percent, the overall effect of SO_2 absorption of solar radiation on UV climatology is likely negligible for all stations except Kagoshima.

The relatively large number of cases with SO_2 above 10 DU in Toronto can be explained by local pollution sources. In addition, more frequent sampling at Toronto, where up to five measurements per hour are made, causes short-term increases of SO_2 to be registered.

The high SO_2 amounts observed over Kagoshima are associated with the Sakurajima volcano, which is 10 km southeast of the observation site and one of the few active volcanoes in Japan. The levels of SO_2 observed there can substantially reduce the level of biologically active ultraviolet radiation. For an SO_2 amount of 50 DU the energy of the erythemally weighted UV spectrum is about 25% less than that for the same atmosphere without SO_2. During the five-year period, SO_2 levels of 50 DU or greater were observed on 65 occasions. Other components of volcanic plumes, such as aerosol and dust, also reduce UV irradiance values.

Table 4.1: List of Stations, Periods of Observation, and Number of Days with High SO_2

Station	Period of Observations	Latitude	Longitude	Number of Days with SO_2 ≥10DU (≥20DU)	Percentage of Total Number of Days with UV Observations
Kagoshima	1991-1995	32°N	131°E	236 (125)*	13.04 (6.92)*
Toronto	1989-1995	44°N	79°W	26 (1)	1.08 (0.04)
Montreal	1993-1995	50°N	74°W	3 (0)	0.32 (0.00)
Saturna	1991-1995	49°N	123°W	5 (0)	0.28 (0.00)
Naha	1991-1995	26°N	128°E	2 (0)	0.11 (0.00)
Churchill	1992-1995	58°N	94°W	1 (0)	0.09 (0.00)
Winnipeg	1992-1995	50°N	97°W	1 (0)	0.08 (0.00)
Edmonton	1992-1995	54°N	114°W	1 (0)	0.08 (0.00)
Saskatoon	1990-1995	52°N	107°W	1 (0)	0.05 (0.00)
Sapporo	1991-1995	43°N	141°E	0 (0)	0.00 (0.00)
Tateno	1991-1995	36°N	140°E	0 (0)	0.00 (0.00)
Halifax	1992-1995	45°N	64°W	0 (0)	0.00 (0.00)
Regina	1994-1995	50°N	105°W	0 (0)	0.00 (0.00)

** Number of days with SO_2 ≥ 20DU and number of such days as a percentage of total number are shown in brackets.*

The long-term effect of volcanic SO_2 absorption on UV climatology at the surface may be estimated by multiplying the number of days with high SO_2 by the reduction of UV irradiance due to SO_2. For Kagoshima this is about a 1–2% reduction. The overall effect of the volcano on UV irradiance is likely stronger, however, because other volcanic plume components absorb and scatter solar radiation. The effect would be at least twice as strong if the observatory were located in the path of the prevailing wind from the volcano. However, since no other Japanese stations report SO_2 values more than 20 DU, it is likely that the effects of this volcano are not widespread.

4.2.3 Dependence on Clouds

The effects of clouds on UV-B may be approached by first investigating their effects on irradiance measurements made at 324 nm, a wavelength that is not significantly affected by ozone or SO_2 absorption, Figures 4.8b and 4.8d show the logarithm of UV irradiance normalized to the irradiance value at 324 nm as a function of wavelength and time of day for May 7, 1992 (Figure 4.8b) and May 6, 1992 (Figure 4.8d). Ozone amounts were approximately the same for both days, but cloud conditions were quite different. Figures 4.8a and 4.8c, which show the absolute irradiance for the two days, indicate a significant drop in irradiance values on the afternoon of May 6. The variations of irradiance on May 6 are due to variations in cloud cover. However, as shown in Figures 4.8b and 4.8d, the behaviour of the ratios for these two days is similar. This illustrates that the effects of clouds on global irradiance are approximately the same for all wavelengths in the UV-B.

For most cases the presence of clouds does not affect the retrieval of total ozone values, since the shape of the normalized spectra are nearly unaffected (Figure 4.8b and 4.8d). However, when very thick cumulonimbus clouds are present the shape of the normalized spectra are affected significantly. Figure 4.8f shows the normalized spectra for May 2, 1992, a day when irradiance values at 324 nm dropped to about 1% of the values for clear sky conditions during the passage of thunderstorms. Calculations during these events yield very high levels of ozone (up to 1000 DU). These effects have been reported earlier by Brewer and Kerr [1973] and are likely caused by very long optical path lengths due to extensive scattering in the clouds.

Information about cloud conditions can be obtained from the absolute value of irradiance at 324 nm. Figure 4.9 shows percentiles of irradiance at 324 nm as a function of zenith angle, derived using data from seven stations. Measured values of irradiance at 324 nm may be compared with the curves in Figure 4.9 to estimate cloud thickness. An observation above the 95th percentile curve would be considered to have been made under clear sky conditions. Observations below the 5th percentile curve would have been made under heavy convective clouds. In terms of absolute values of irradiance, the 5th percentile level corresponds to 12–15% of irradiance at 324 nm for clear sky conditions. Values of irradiance at 324 nm under the 1st percentile level are probably from measurements made under very thick cumulonimbus clouds.

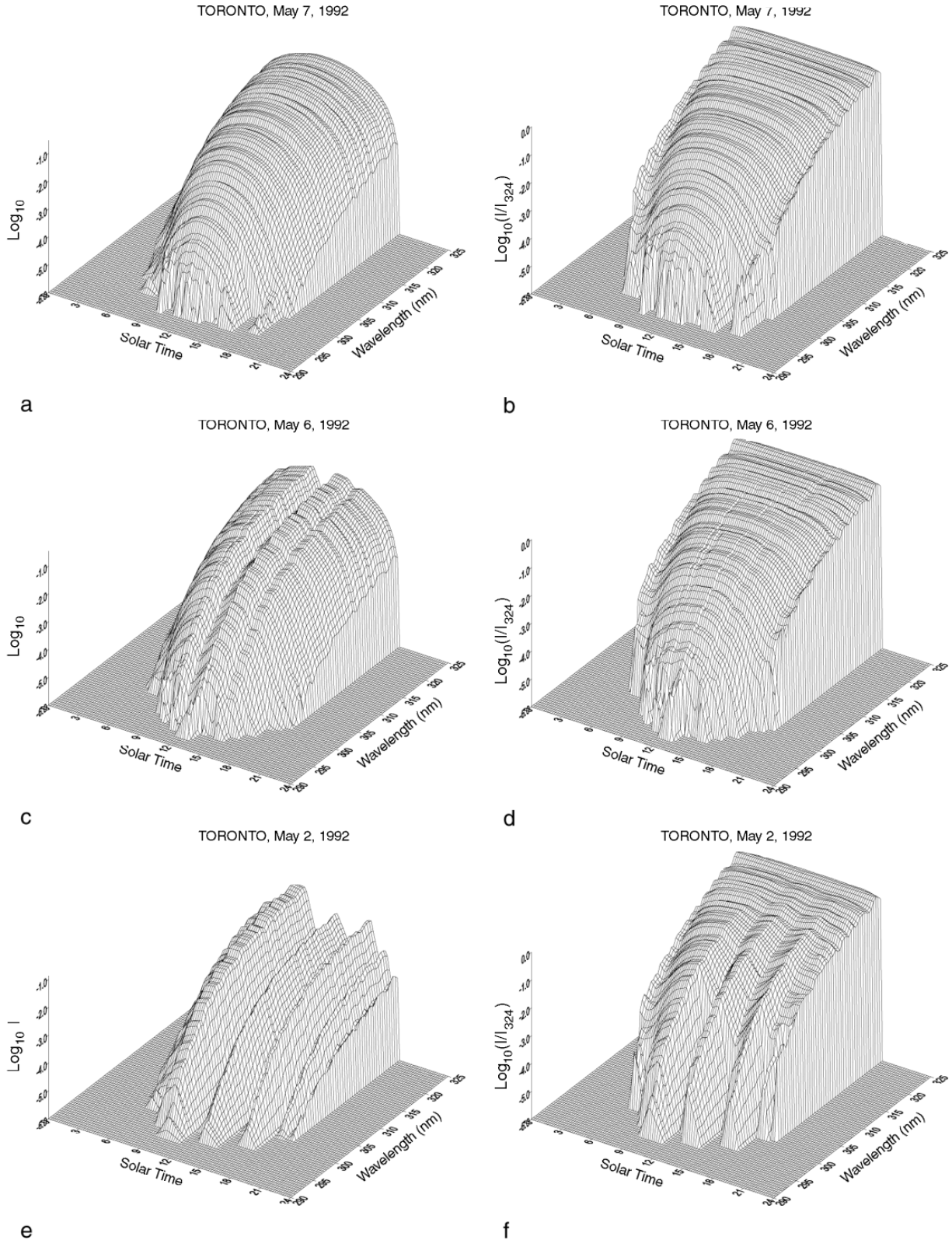

Figure 4.8 The logarithm of the UV irradiance (a, c, e) and the logarithm of UV irradiance normalized to the irradiance value at 324 nm (b, d, f) as a function of wavelength and time of day for May 2, 6, and 7, 1992.

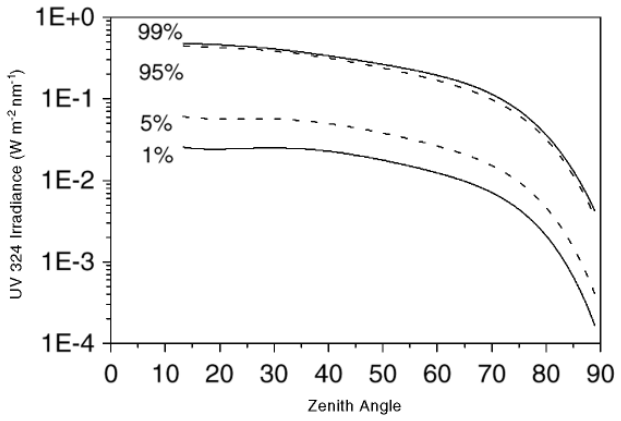

Figure 4.9 Percentiles of UV 324 nm irradiance distribution as a function of zenith angle (the 1% or 1st percentile means that 1% of the observations is below this curve).

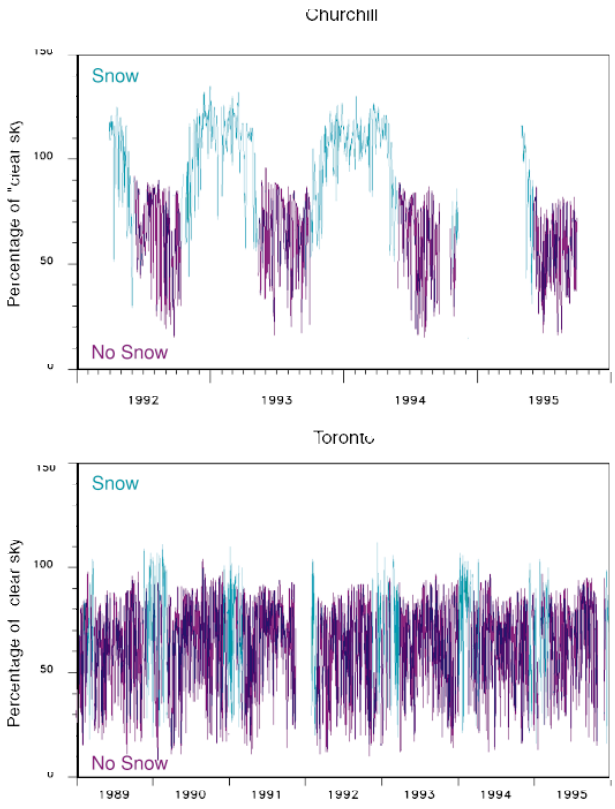

Figure 4.10 Averages of the daily mean adjusted UV 324 nm irradiance for days with and without snow on the ground for Churchill (60˚N) and Toronto (44˚N).

4.2.4 Dependence on Other Variables

UV irradiance depends on surface albedo, and snow on the ground is the main factor that affects surface albedo in the UV. To estimate the effect of snow on UV irradiance, all Canadian Brewer observations taken under clear sky conditions have been divided into two groups: those taken with snow on the ground and those taken without. Data were used only for conditions when no clouds were reported at nearby weather stations. UV irradiance at 324 nm was used as an indicator of the UV signal. The effect of zenith angle was removed by dividing the UV irradiance values at 324 nm by the 95th percentile value (see Figure 4.9) at the corresponding zenith angle. The daily average of these values represents a relative level of UV irradiance adjusted for zenith angle and is called the "adjusted UV 324 nm irradiance."

Table 4.2 summarizes the averages of the adjusted UV 324 nm irradiance for clear days with and without snow on the ground for seven Canadian Brewer stations. An important result that is evident here is that for clear sky and no-snow conditions the adjusted UV 324 nm irradiance is similar at all stations and snow has significantly different enhancements at different stations likely because of terrain variations.

Figure 4.10 shows the daily average adjusted UV 324 nm irradiance values for all days at Churchill and Toronto. Days with snow (blue) have generally higher values than days without snow (red). The difference between "snow" and "no snow" is more apparent at Churchill, where the nearby flat terrain is likely "whiter" than at Toronto, which has urban surroundings.

The presence of atmospheric aerosols affects the amount of global UV irradiance at the ground. In a study by Kerr [1997], data from clear days over a three-year period (1989–1991) at Toronto were used to quantify the effect of aerosols on UV-B irradiance values. Variations in irradiance values measured with the Brewer instrument were compared with aerosol optical depth measurements for UV-B wavelengths made with the same instrument. The analysis found that aerosols reduce the global irradiance by about 20–30% of the reduction of the direct irradiance. (Thus, if aerosols were to reduce the direct irradiance by 10%, the global irradiance would be reduced by 2–3%.) The reduction has little wavelength dependence and is in reasonable agreement with radiative transfer models for non-absorbing aerosols.

Table 4.2: Averages of the Adjusted UV 324 nm Irradiance for Clear Days With and Without Snow on the Ground

Station	No snow	Snow	Difference (% from "no snow" level)
Resolute	82	111	35
Churchill	84	116	39
Edmonton	84	103	21
Winnipeg	87	111	27
Montreal	80	97	22
Halifax	86	93	8
Toronto	85	95	12

4.2.5 Modelling of Spectral UV Irradiance

Radiative transfer models [e.g. Dave 1964; Stamnes et al. 1988] can be used to estimate spectral UV irradiance from a number of measured parameters, such as total ozone and aerosol and cloud conditions. For clear sky conditions, systematic differences between measurements and models are typically in the order of several percent [Mayer et al. 1997]. These differences are mostly due to errors in the model input parameters (e.g., extraterrestrial radiance) and uncertainties in the absolute calibration and characterization of the spectroradiometer [Mayer et al. 1997]. However, differences between individual measurements and the modelled radiation can be much higher. According to Schwander et al. [1997], typical errors in the input parameters can lead to a 10–20% uncertainty in the global UV irradiance at 300 nm and up to 50% uncertainty at 290 nm. If ozone and SO_2 contents and spectral aerosol characteristics are measured under actual conditions, the uncertainties in input parameters result in an uncertainty of about 5% for spectral integrals of UV irradiance [Schwander et al., 1997].

4.3 Changes in UV Irradiance due to Ozone Depletion

The extent to which ozone has been decreasing over the past two decades has been reported by many researchers, and the results have been summarized in periodic international scientific assessments [e.g., WMO 1991; 1994]. Depletion of stratospheric ozone over Canada has been summarized in Chapter 1 of this report. These assessments have quantified the long-term trends in ozone as a function of latitude and time of year and have summarized findings that relate these changes to enhanced levels of anthropogenic chlorine and bromine in the stratosphere. The long-term trend values are based on the results of analyses of stratospheric ozone measurements that have been made routinely on a global scale for nearly four decades.

Quantifying long-term changes in UV irradiance at the earth's surface is more difficult than detecting long-term changes in ozone, since surface UV irradiance depends on many variables. Although analysis of spectral data can separate changes due to ozone from changes due to other causes (Section 4.1), it is only relatively recently (since the late 1980s) that instruments have been developed with the capability of carrying out routine field measurements of spectral UV irradiance with sufficient accuracy and long-term stability.

4.3.1 Analysis of UV Irradiance Records

Relatively short records of spectral UV irradiance have been studied to determine possible increases that may be caused by decreases in stratospheric ozone. Kerr and McElroy [1993, 1994] analysed daily integrated UV irradiance values and total ozone measured at Toronto between 1989 and 1993 and found significant increases in UV irradiance resulting from a large drop in ozone over the same period. Data from all days were used, so the analysis includes the effects of clouds and other variables. The decrease in ozone occurred mostly in 1993 and was associated with the volcanic eruption of Mt. Pinatubo in June 1991. These significantly perturbed conditions provided an opportunity to quantify the links between changes in UV irradiance and changes in ozone and to demonstrate through the spectral signature that the UV changes were caused by ozone. Figure 4.11 shows the ratios of data from a year with low ozone (1992-1993) to a year with higher ozone (1989-1990) for summer (May to August) and winter (December to March) and compares these ratios with the absorption spectrum of ozone. The spectral absorption features of ozone are clearly evident in the temporal changes in UV irradiance. The study is important because it demonstrates the capability to observe these absorption features in data gathered under all types of weather conditions.

The analysis of the Toronto data set has been extended both into the past (from 1989 to 1986) and into the future (beyond 1993 to 1997). Data prior to 1989 are not as reliable as later data, since the measurements were made over a reduced wavelength range (290–315 nm) and there is more uncertainty in the absolute calibration of the instrument. Nevertheless, when the longer data set (now with 11 years of data) is analysed to determine long-term changes, the relationship of changes in UV irradiance to changes in ozone remains very clear. Figure 4.12a shows the summer daily average values of irradiance at 300 nm (where ozone absorbs strongly) and 324 nm (where ozone has negligible absorption). UV irradiance values from 315 nm to 325 nm prior to 1989 have been calculated from data between 290 nm and 315 nm and the very strong statistically determined correlations between irradiance at the shorter and longer wavelengths. The

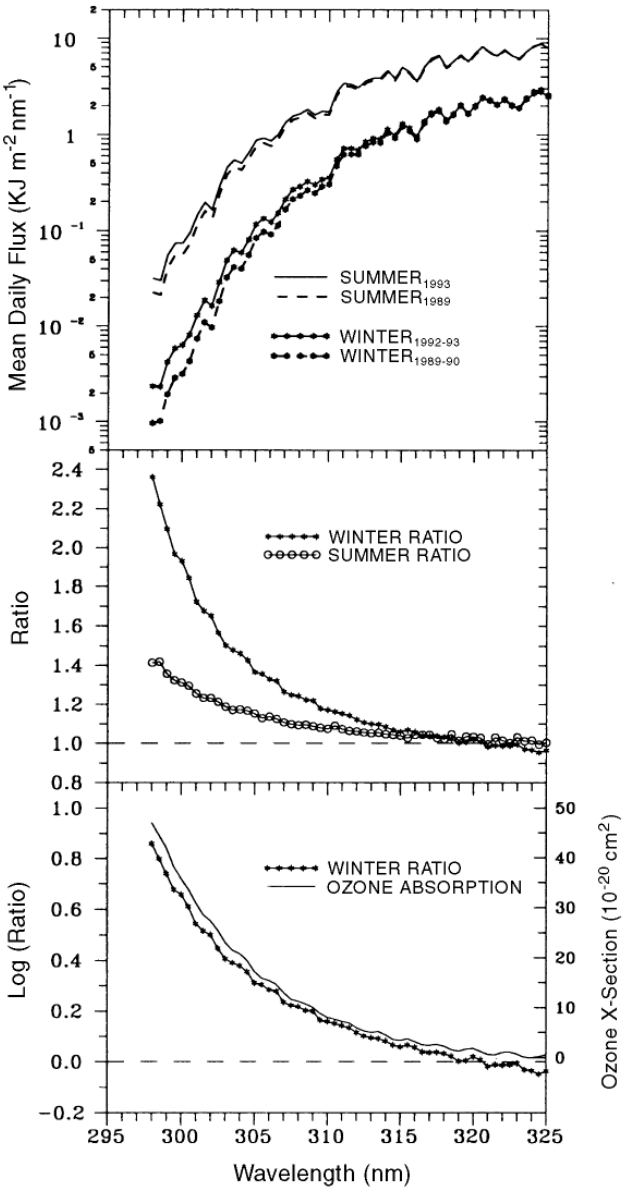

Figure 4.11 Impact of low ozone over Toronto in 1992 and 1993 compared with earlier years. The top panel shows the main daily UV flux as a function of wavelength for the summers of 1989 and 1993 and the winters of 1989–1990 and 1992–1993. The middle panel shows flux ratios for summer (1993 divided by 1989) and for winter (1992–1993 divided by 1989–1990). The bottom panel compares the observed changes as a function of wavelength with the ozone absorption spectrum. The log of the winter ratio is used because the intensity of UV-B radiation depends on the exponent of the absorption coefficient of ozone. (From WMO [1994].)

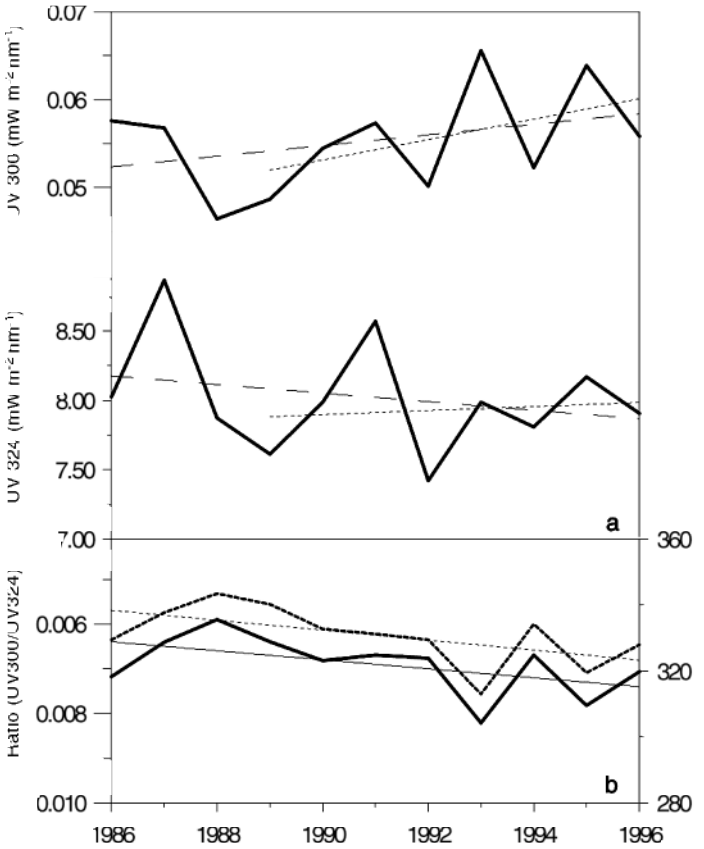

Figure 4.12. (a) The summer daily average values of irradiance at 300 nm (where ozone absorbs strongly) and 324 nm (where ozone has negligible absorption). (b) The ratio between the average daily integrated value of UV irradiance at 300 nm to that at 324 nm for the summer months (May–August). Seasonal mean total ozone is shown by the dotted line. The best fit lines are also plotted.

accuracy of the proxy data at 324 nm is estimated to be about 5% for an individual scan and about 2% for the summertime averages prior to 1989. Both data sets have been fitted with two trend lines: one from 1986 and the other from 1989. The linear fits show a positive trend at 300 nm and near zero (since 1989) or negative (since 1986) at 324 nm. The slopes of the trend lines as a function of wavelength for the data since 1989 are shown as percent per decade in Figure 4.13, with the ozone absorption spectrum for comparison.

Figure 4.12b shows the ratio of irradiance at 300 nm to that at 324 nm (on a decreasing scale) and the average summer total ozone value for each year. The relationship between the average ratio of irradiance at 300 nm to that at 324 nm and average total ozone values is quite evident on a year-to-year as well as a longer-term basis.

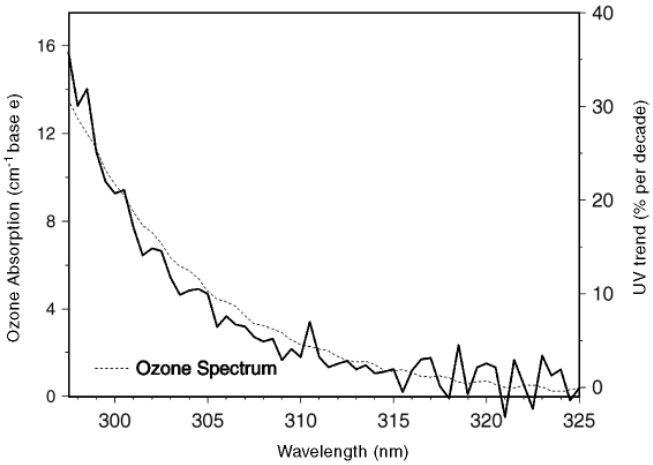

Figure 4.13 UV irradiance trends for May–August for Toronto. The slopes of the trend lines as a function of wavelength for the data from 1989 to 1996 are shown as percent per decade with the ozone absorption spectrum.

4.3.2 Present UV Climatology

There are now about 100 station years of spectral UV irradiance data stored in the WOUDC. Many of the stations have records more than five years long. These data have been used to determine average UV values measured over the length of the records at each site. One example of how these UV "climatologies" may be graphically summarized is shown in Figure 4.14. In this example, the average values of the observed UV Index [Kerr et al. 1994; Burrows et al. 1994; Burrows 1997; see also Section 4.4] are shown as a function of time of day and time of year at Churchill, Canada (59°N), San Diego, USA (32°N), Toronto, Canada (44°N), and Sapporo, Japan (43°N).

Inspection of the diagrams in Figure 4.14 reveals several interesting aspects of UV irradiance. At San Diego, Toronto, and Sapporo, the UV Index is lower near the spring equinox (March 21) than it is near the fall equinox (September 21). This is due to the fact that there is more ozone during spring than there is in fall. In Churchill, however, the UV Index is higher in spring than it is in the fall. This is because the UV levels are enhanced by snow on the ground, which usually disappears in May. Comparison of the four station climatologies clearly shows enhanced UV irradiance at lower latitudes. It also illustrates longer hours of sunshine during summer and shorter hours during winter at high latitudes. Comparison of the climatology at Toronto with that at Sapporo indicates that there can be significant differences in UV levels at two stations with similar latitude. These differences are due to different ozone and/or cloud conditions.

The measured climatologies that are evolving from the growing data base are useful for the study of short-term variations. Figure 4.15 shows the UV Index for individual years at Toronto (44° N, 1993), Ushuaia, Argentina (54° S, 1994), Palmer, Antarctica (64° S, 1993), and Mauna Loa, Hawaii (20° N, 1997). The observed day-to-day fluctuations are much larger than one might infer from the climatology diagrams shown in Figure 4.14. These fluctuations result in larger peak values than are seen in the climatological averages. For example, the climatology for Toronto shows a peak Index of less than 7 in June and July, but the individual observations made in 1993 (when ozone was a record low) show peak values of about 9.5. Figure 4.15 shows that Palmer under the ozone hole in October has UV Index values greater than 10, suggesting very strong sun-burning potential there. The record at Mauna Loa shows that the combination of typically low tropical ozone values with high sun angles and high altitude can result in UV Index values peaking near 16.

4.3.3 Estimating Past UV Climatology

In order to determine long-term changes in UV irradiance that may have occurred since the onset of ozone depletion in the late 1970s, it is necessary to estimate levels of UV irradiance that existed before routine spectral measurements were made. Estimates of past UV levels are the product of a thorough understanding of the dependencies of spectral UV irradiance on geophysical variables (Section 4.1) and the application of these relationships with the aid of radiative transfer models to archived measurements of other variables (e.g., ozone, cloud cover, optical depth, etc.). Work towards reconstructing past UV climatology has been initiated in recent years. These estimated past climatologies may then be compared with those of recent years (Section 4.3.2) to determine long-term changes.

Several studies have been done [e.g., Frederick et al. 1993; Madronich 1992] that calculate changes in UV irradiance from long-term changes in total ozone measured by ground-based or satellite instruments. In deriving estimated changes in UV irradiance, most of these studies have assumed that the effects of clouds and other variables have not changed over time and are therefore representative of changes under clear sky conditions.

More recently Herman et al. [1996] have estimated past UV irradiance values at the surface from measurements made by the Total Ozone Mapping Spectrometer (TOMS). The TOMS instrument uses backscattered radiance measurements at several wavelengths in the UV to determine total ozone from space. The backscattered data may also be used to estimate

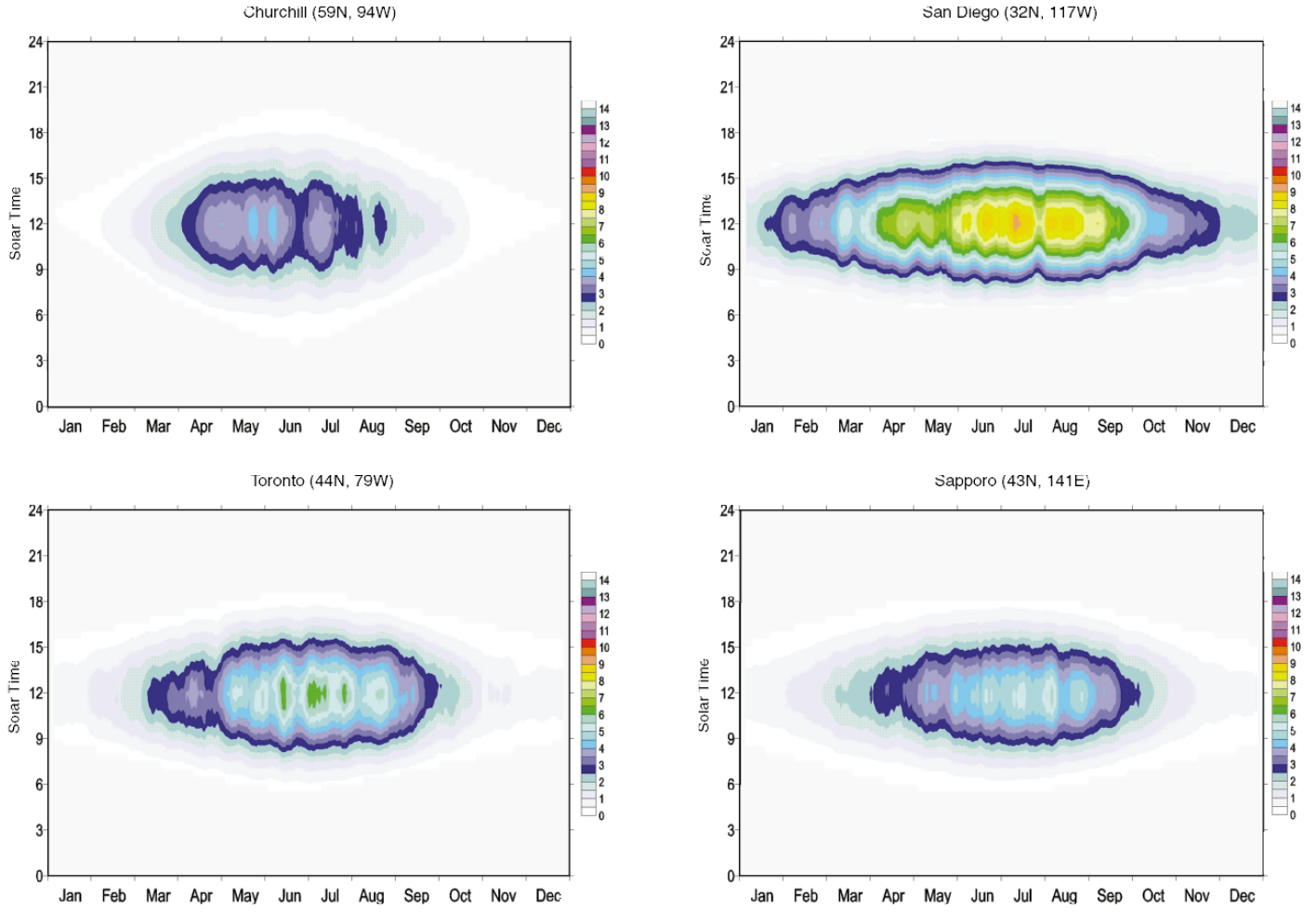

Figure 4.14 UV Index "climatology" for San Diego, Churchill, Toronto, and Sapporo.

cloud thickness and therefore derive the attenuation of surface UV irradiance due to clouds. Comparison of the TOMS-estimated UV surface irradiance with actual ground-based irradiance measurements has played a key part in the development of this approach [Eck et al. 1995]. Although there are still problems to overcome with this method, the potential to provide a realistic estimation of surface UV irradiance values on a daily basis with global coverage back to the late 1970s is quite promising. The possibility of extending the record further back in time at sites where total ozone and cloud cover are measured also exists, although results of such analyses are yet to be reported.

4.4 The Contribution of Ozone-Depleting Gases to Global Warming

The anthropogenic emission of chlorine-bearing gases into the atmosphere has resulted in a significant depletion of the earth's ozone layer and the development of the Antarctic ozone hole. Many of these gases are also strong greenhouse gases that modify the atmospheric radiation so as to make the earth's surface warmer and the stratosphere colder. This is particularly true of CFC-11 and CFC-12, but new alternatives to CFCs, such as HCFC-22 (designed for the replacement of CFC-11 and CFC-12) are also strong greenhouse gases, even though they may not deplete as much ozone. The buildup of carbon dioxide and other greenhouse gases contributes to cooling of the polar stratosphere, which favours the formation of Polar Stratospheric Clouds (PSCs) [Austin 1992]. Consequently, the accumulation of these gases may have increased the severity of ozone depletion in the Antarctic ozone hole

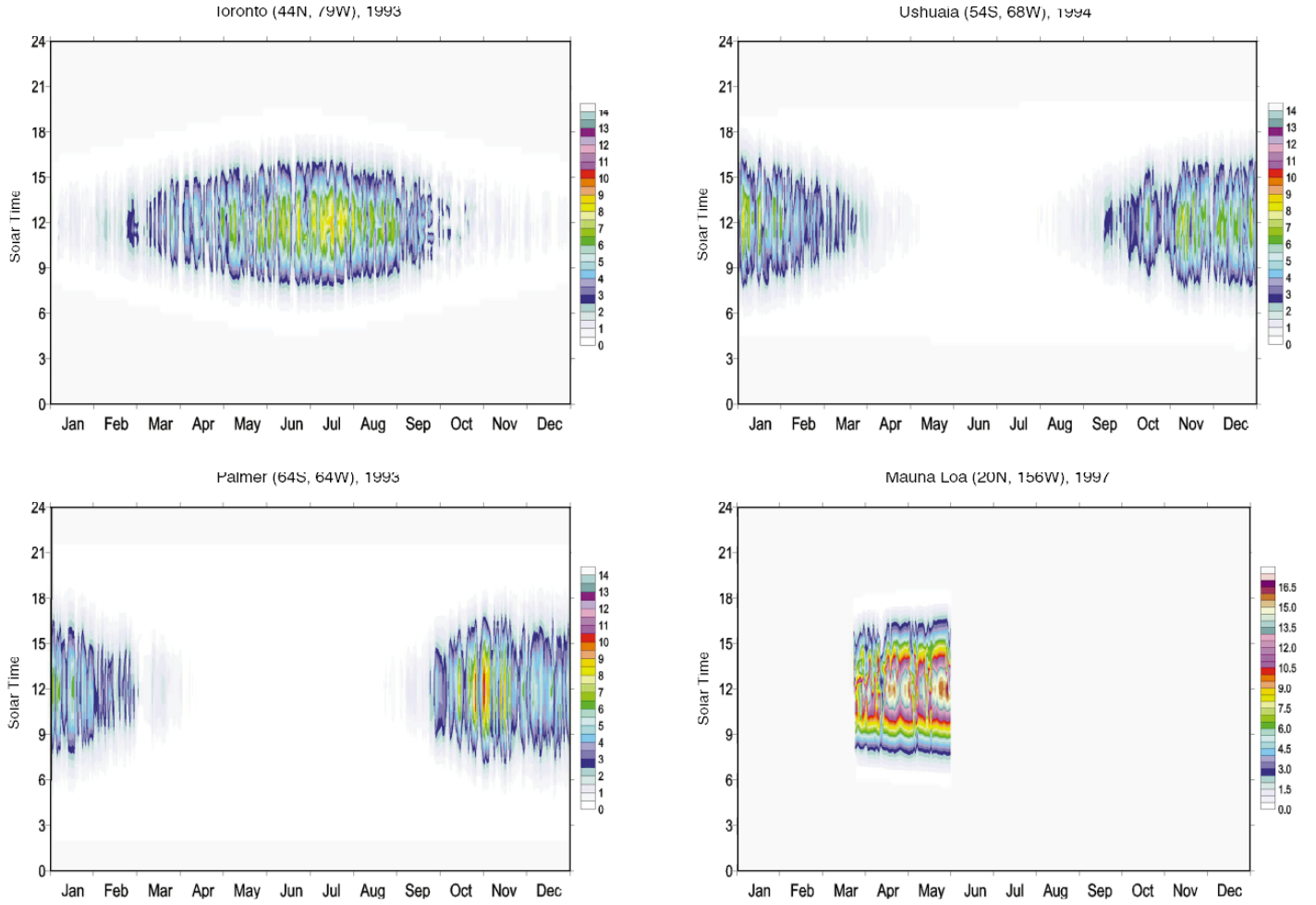

Figure 4.15 The UV Index for individual years at Toronto (44°N, 1993), Ushuaia, Argentina (54°S, 1994), Palmer, Antarctica (64°S, 1993), and Mauna Loa, Hawaii (20°N, 1997).

and enhanced Arctic ozone depletion in late winter. In addition, the increase in atmospheric methane concentrations has increased the amount of water vapour in the stratosphere, thus probably enhancing polar ozone depletion by making more water available for PSC formation. The depletion of the stratospheric ozone layer will also cause surface cooling in the polar regions, as discussed later in this section. Hence, the greenhouse gases contribute indirectly in a variety of ways to ozone depletion, which itself mitigates global warming.

In order to evaluate the contributions of the various gases to global warming, the concept of radiative forcing or changes in absorption of the upward long-wave radiation by the atmosphere has been formulated [Ramanathan 1987; IPCC 1994]. Using the radiative forcing at the tropopause as an input, climate models can then estimate the effect of these gases on global temperature. Model calculations of this radiative forcing and the associated fluxes have been conducted by several authors [Dickinson and Cicerone 1986]. Earlier estimates of the greenhouse effect were expressed in terms of the overall loss of radiation to space or of the downward radiation at the surface. It may be noted that, when convection just above the ground is small, the land surface temperature actually responds to the downward greenhouse radiation from the atmosphere in a few hours. The greenhouse radiation is typically about 150 Wm^{-2}; the modelled increases in the greenhouse radiation since pre-industrial times are about 2.2 Wm^{-2}. The increase in downward surface greenhouse radiation for a particular gas is quite similar to the absorption of upward long-wave radiation by that gas, as has been demonstrated by Sinha and Toumi [1996]. Estimates of the radiative fluxes at the tropopause from greenhouse gases at current 1997 concentrations are given in Table 4.3. These are based on the 1990 IPCC report [IPCC 1990]. Although there are extensive model calculations of radiative forcing in the literature, there are few experimental measurements. In what follows, measurements of the surface greenhouse radiation are described and compared with estimates from radiative transfer modelling.

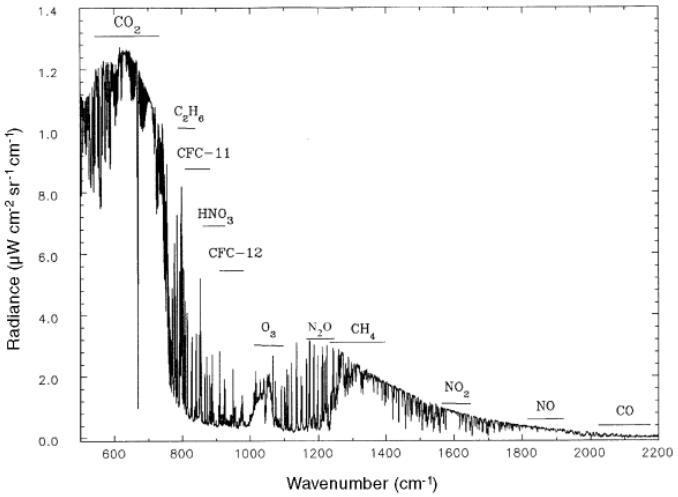

Figure 4.16 A spectrum of downward (greenhouse) radiation at the surface, showing the contributions of several greenhouse gases observed at Peterborough, Ontario, in February 1996.

Table 4.3: Radiative Fluxes at the Tropopause (after IPCC [1990])

Greenhouse Gas	Simulated Flux (Wm^{-2})
H_2O	~90
CO_2	56
CH_4	1.51
N_2O	2.48
Tropospheric O_3	0.70
CFC-12	0.15
CFC-11	0.062

Table 4.4: Measured Greenhouse Fluxes at the Earth's Surface

Greenhouse Gas	Emission Band (cm^{-1})	Measured Flux (Wm^{-2})	Simulated Flux (Wm^{-2})
CFC-11	830–860	0.13	0.12
CFC-12	900–940	0.10	0.090
CFC-12	all bands	0.24	0.22
CFCs-11 & 12	all bands	0.37	0.34
CCl_4	786–806	0.046	0.039
HCFC-22*	780–830	NA	0.030
HNO_3	850–920	0.085	0.060
N_2O	all bands	1.33	1.30
CH_4	1200–1400	0.85	0.80
CO	2000–2200	0.032	0.033
CO_2*	all bands	NA	60.9
O_3	950–1100	6.52	6.39
Tropospheric O_3	950–1100	0.11	0.07

* *greenhouse flux is based on simulations only*

A project to measure the increases in greenhouse radiation at the surface has been conducted at a location in Ontario for the past five years. Measurements of the fluxes from the individual gases CFC-11, CFC-12, CCl_4, CH_4, N_2O, HNO_3, CO, and tropospheric ozone have been reported in a series of papers by Evans and Puckrin [1994–1997]. The measurements were made with a standard Fourier-transform infrared (FTIR) spectrometer operated at a resolution of 0.25 cm^{-1}. The investigation has focused on those radiatively active gases that may have a particularly large adverse effect on climate, either because of their high atmospheric concentrations, their large global warming potentials, or a combination of these factors. Figure 4.16 shows a typical spectrum of the downward radiance in the 8–12 μm wavelength range and identifies emissions from several of the greenhouse gases.

The greenhouse radiation from tropospheric ozone was measured by a technique in which the base of cold clouds is used as a cold target. The thermal emission from the warm atmosphere below the cloud is measured against the low background emission from the cold cloud base [Puckrin et al. 1996]. The cloud also screens out the emission from the stratospheric ozone above it. The greenhouse emission from tropospheric ozone in the lower 2 km and the lower 4 km of the atmosphere has been measured at about 0.1 Wm^{-2} on several occasions.

The downward radiation fluxes at the surface from those greenhouse gases measured to date are summarized in Table 4.4. The measurements, except for tropospheric ozone, were made in clear sky, winter conditions at latitude 44°N. The values in Table 4.4 are for average sky conditions, assuming that the sky is overcast 50% of the time. They are 50% of the measured (clear sky) values and can be compared with IPCC values, which generally include the effects of cloud cover. The measurement pertaining to tropospheric ozone was made in moderately polluted air with an ozone concentration of 60 ppbv. Fluxes predicted by the FASCD3 atmospheric transmission code [Anderson et al. 1986] for the actual atmospheric conditions and recent atmospheric gas concentrations [Kaye et al. 1994 ; IPCC 1995] are also shown in Table 4.4. In general there is a good correlation between the measured and simulated radiative fluxes. Only nitric acid and tropospheric ozone show significant deviations between the measured and simulated flux values.

The flux measurements presented in Table 4.4 provide important experimental verification of the radiation that is responsible for global warming and that may be introducing significant changes in the climate system. Continued measurements of the downward greenhouse fluxes over a range of locations and seasons would provide useful information for validating global climate models and resolving the discrepancies that currently exist between them. For example, a

Table 4.5: Contribution of Greenhouse Gases to the Surface Downward Flux Since the Pre-industrial Era

Greenhouse Gas	Pre-industrial Concentration	Current Concentration	Flux Increase (Wm^{-2})	%
Carbon dioxide	275 ppmv	360 ppmv	1.30	60 %
Methane	0.7 ppmv	1.75 ppmv	0.33	15 %
Nitrous oxide	285 ppbv	316 ppbv	0.13	6 %
Tropospheric ozone	30 ppbv	60 ppbv	0.04	2 %
CFC-11	0 pptv	280 pptv	0.13	6 %
CFC-12	0 pptv	530 pptv	0.24	11 %
Total	.	.	2.17	100 %

comparison of surface fluxes from 20 models conducted by Ellingson et al. [1995] reported only the CO_2 fluxes, although the combined CH_4 and N_2O flux were reported for one model. That model's reported value of 1.7 Wm^{-2} is broadly consistent with the experimental value of 2.1 Wm^{-2}.

Table 4.5 shows the contribution of greenhouse gases to the increase in the downward greenhouse flux since the pre-industrial period. Simulations using FASCD3 were performed to estimate the greenhouse flux from the various gases, using their respective tropospheric concentrations from two centuries ago [Dickinson and Cicerone 1986]. Most of the simulations of the current fluxes have been verified with the experimental measurements in Table 4.4, so that there is some confidence that these modelled flux increases are representative of Canadian latitudes. In these calculations, the amount of atmospheric water vapour has been assumed to be invariant.

The pre-industrial and current concentrations of gases used in the flux calculations are also summarized in Table 4.5. The current tropospheric ozone amount of 60 ppbv over the first 2 km of the atmosphere is typical of a moderately polluted environment. From Table 4.5 it is apparent that the increase in the carbon dioxide concentration since pre-industrial times has resulted in the largest increase in the radiative forcing at the surface. The chlorofluorocarbons, CFC-11 and CFC-12, contribute the second largest amount to the flux; however, carbon dioxide has increased about 100,000 times more than the combined concentrations of CFC-11 and CFC-12 since the pre-industrial period. The data from Table 4.5 are represented pictorially in Figure 4.17a, which shows the relative contribution of greenhouse gases to the downward greenhouse flux since the pre-industrial period.

Radiative forcing at the tropopause, as taken from IPCC [1995], is shown in Table 4.6 and Figure 4.17b. These radiative forcing contributions are more representative of global averages, although they are of the same magnitude as the surface flux increases in Table 4.5. The estimated total radiative forcing is 2.92 Wm^{-2} with an uncertainty range of 2.4–3.5 Wm^{-2}.

The contribution of water vapour to the increase in greenhouse radiation has not been included, since it is a part of the natural climate feedback. It is possible that tropospheric water vapour has already increased by several percent. The water vapour flux is typically about 90 Wm^{-2}, giving a total greenhouse radiation of about 150 Wm^{-2}. From Table 4.5 it is evident that the greenhouse radiation has increased by about

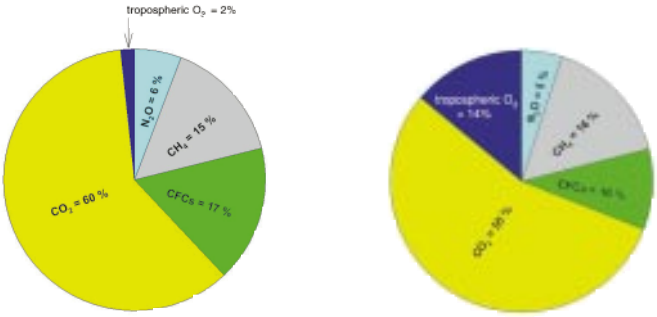

Figure 4.17 (a) Percentage increases in measured surface radiation. (b) Percentage increases in radiative forcing. (From IPCC [1995].)

Table 4.6: Contribution of Greenhouse Gases to Radiative Forcing Since the Pre-industrial Era (after IPCC [1995])

Greenhouse Gas	Pre-industrial Concentration	Current Concentration	Flux Increase (Wm^{-2})	%
Carbon dioxide	275 ppmv	360 ppmv	1.6	55 %
Methane	0.7 ppmv	1.75 ppmv	0.48	16 %
Nitrous oxide	285 ppbv	316 ppbv	0.14	5 %
Tropospheric ozone	25 ppbv	60 ppbv	0.4	14 %
CFCs	0 pptv	1ppbv	0.3	10 %
Total			2.92 (2.4–3.5)	100%

2.2 Wm^{-2} since pre-industrial times. Of this 2.2 Wm^{-2}, nearly 0.5 Wm^{-2} has been attributed by measurements to CFCs. The CFC contribution is mainly due to CFC-11, CFC-12, CCl_4, CFC-22, and CFC-113.

In Table 4.7 some of the factors that may produce cooling of the climate are considered [IPCC 1995]. These cooling factors are important because they may partially compensate for the observed increases in greenhouse radiation and radiative forcing. The depletion of stratospheric ozone causes cooling in the polar regions but not in the tropics. This is because stratospheric ozone both attenuates solar UV radiation that heats the surface and emits infrared (IR) radiation that also heats the surface. If the ozone layer is thinned, more solar UV radiation reaches the surface to heat it but less long-wave IR is emitted. If the long-wave term is larger, its reduction will therefore lead to cooling at the surface. In the winter polar regions, for example, a thinning of the ozone layer causes net cooling of up to 0.2 Wm^{-2} since the short-wave solar UV is very small in this situation. In the tropics the solar UV term is larger, and consequently an ozone thinning actually causes a net heating of the surface of 0.05 Wm^{-2}.

Table 4.7: Cooling Influences (after IPCC [1995])

Stratospheric ozone depletion (5 %)		–0.05 to +0.2 Wm^{-2}
Sulfate aerosols	direct	0.2 to 0.8 Wm^{-2}
	indirect	0 to 1.5 Wm^{-2}
Solar variability		–0.1 to –0.5 Wm^{-2}

4.5 Public Awareness Programs

Environment Canada runs two public awareness programs dealing with ozone conditions: Ozone Watch, which reports current ozone measurements, and the UV Index Program, which gives forecasts of UV radiation.

Ozone Watch was started in March 1992, largely in response to public concerns about low ozone values in the Arctic. The reports are based on measurements at the twelve Canadian Brewer locations. A single percentage is given for each location, describing the mean ozone value over the preceding two weeks in relation to pre-1980 average values. The goal of the program is to present a rough indication of ozone depletion and to show interested people that ozone changes in much the same way as other atmospheric variables. Ozone Watch is put on the wire service every Friday in tabular form. It is also issued as a map with spot values, shown on a commercial weather service (Meteomedia), and posted on an Environment Canada Web site. It is believed to be unique to Canada, and it often generates questions from journalists who may notice low ozone values earlier than anyone else. The Ozone Watch ensures that Environment Canada is not ever seen to be withholding data on ozone.

The UV Index program was started in May 1992. It predicts the strength of UV erythemally weighted irradiance, using a number describing the maximum irradiance that will occur on a given day. The forecast is issued the previous evening and is carried on radio and television and in newspapers. The UV Index itself is an irradiance scale, computed by multiplying the CIE irradiance in Wm^{-2} by 40. Thus, the clear sky value at sea level in the tropics would normally be in the range 10–12 (250–300 mW m^{-2}), while 10 would be an exceptionally high value for northern mid-latitudes. This scale has been adopted by the WMO and WHO and is in use in a number of other countries. UV intensity is also described in terms of ranges running from low (values less than 4) to medium (4–7), high (7–9), and extreme (9+). Media reports use these descriptors as well as actual index values. UV Index forecasts that are sent to the regional offices of Environment Canada list the periods when the index is predicted to be in the highest range. Televised reports on Meteomedia's Weather Channel show a predicted index curve throughout the day and add measured values from local radiometers run by Meteomedia as the observations become available.

The UV forecasts are produced from measurements of ozone on the current day and the output from the Numerical Weather Prediction (NWP) model of the Canadian Meteorological Centre. First, the ozone field is predicted using current (real-time) ozone measurements from the Canadian Brewer network and a statistically derived relation between ozone and the NWP output. The clear sky value at the CIE irradiance is then computed from the predicted ozone. Finally, the clear sky value is adjusted for the expected sky conditions using a statistical prediction of sky cover [*Burrows, et al.,* 1994].

References

Anderson, G.P., S.A. Clough, F.X. Kneizys, J.H. Chetwynd, and E.P. Shettle, 1986. *AFGL Atmospheric Constituent Profiles (0–120 km)*, AFGL-TR-86-0110. Cambridge, Mass.: Air Force Geophysical Laboratory.

Austin J., N. Butchart, and K.P. Shine, 1992. Possibility of an Arctic ozone hole in a doubled-CO_2 climate. *Nature,* **360,** 221–225.

Basher, R.E., 1982. *Review of the Dobson spectrophotometer and its accuracy*. WMO Ozone Rep. 13. Geneva: World Meteorological Organization.

Bojkov, R.D., V.E. Fioletov, and S. B.Diaz, 1995. The relationship between solar UV irradiance and total ozone from observations over southern Argentina. *Geophys. Res. Lett*, **22**, 1249–1252.

Brewer, A.W., and J.B. Kerr, 1973. Total ozone measurements in cloudy weather. *Pure Appl. Geophys.,* **106–108**, 928–937.

Burrows W., 1997. Cart regression models for predicting UV radiation at the ground in the presence of cloud and other environmental factors. *J. Appl. Meteorol*., **36**, 531–544.

Burrows, W., M. Vallee, D.I. Wardle, J.B. Kerr, L.J. Wilson, and D.W. Tarasick, 1994. The Canadian UV-B and total ozone forecast model. *Met. Apps.,* **1**, 247–265.

Dave, J.V., 1964. Meaning of successive iteration of the auxiliary equation of radiative transfer. *Astrophysics J.,* **140,** 1292–1303.

deGruijl, F.R., and J.C. van der Leun, 1994. Estimate of the wavelength dependency of ultraviolet carcinogenesis in humans and its relevance to risk assessment of stratospheric ozone depletion. *Health Physics,* **67,** 319–325.

Dickinson, R.E., and R.J. Cicerone, 1986. Future global warming from atmospheric trace gases. *Nature*, **319**, 109–115.

Eck, T.F., P.K. Bhartia, and J. B. Kerr, 1995. Satellite estimation of spectral UVB irradiance using TOMS-derived total ozone and UV reflectivity. *Geophys. Res. Lett*, **22**, 661-614.

Ellingson, R.G, J. Ellis, and S. Fels, 1991. The Intercomparison of radiation codes used in climate models: long wave results. *J. Geophys. Res*., **96**, 8923–8953.

Evans, W.F.J., and E. Puckrin, 1994a. An observation of the atmospheric emission spectrum of CFC-11. *Geophys. Res. Lett*., **21**, 2381–2384.

Evans, W.F.J., and E. Puckrin, 1994b. An observation of the atmospheric thermal emission spectrum of dichlorodifluoromethane. *Can. J. Appl. Spectrosc*., **39**, 85–90.

Evans, W.F.J., and E. Puckrin, 1995a. An observation of the greenhouse radiation associated with carbon monoxide. *Geophys. Res. Lett*., **22**, 925–928.

Evans, W.F.J., and E. Puckrin, 1995b. The extraction of the thermal emission band of methane from the longwave spectrum of the atmosphere. *J. Climate*, **8**, 3091–3095.

Evans, W.F.J., and E. Puckrin, 1995c. The measurement and extraction of the n6 atmospheric emission band of CFC-12 from interfering emission features. *Ann. Geophysicae*, **13,** 969–972.

Evans, W.F.J., and E. Puckrin, 1996. A measurement of the greenhouse radiation associated with carbon tetrachloride (CCl_4). *Geophys. Res. Lett*., **23**, 1769–1772.

Evans, W.F.J., and E. Puckrin, 1997. A wintertime measurement of the greenhouse radiation from nitrous oxide. *Can. J. Appl. Spectrosc*., forthcoming.

Fioletov, V.E., J.B. Kerr, D.I. Wardle, 1997. The relationship between total ozone and spectral UV irradiance from Brewer observations and its use for derivation of total ozone from UV measurements. Working paper. Atmospheric Environment Service, Downsview, Ontario.

Frederick J.E., P.F. Soulen, S.B. Diaz, I., Smolskaia, C.R. Booth, T. Lucas, and D. Neuschuler, 1993. Solar ultraviolet irradiance observed from Southern Argentina: September 1990 to March 1991, *J. Geophys. Res.,* **98**, 8891–8897.

Götz F. W. P., 1931. Zum Strahlungsklima des Spitzbergen Sommers. *Gerlands Beiträge zur Geophys.*, **31**, 119.

Herman J. R., P.K. Bhartia, J. Ziemke Z. Ahmad, and D. Larko, 1996. UV-B radiation increases (1979–1992) from decreases in total ozone. *Geophys. Res. Lett.,* **23**, 2117–2120.

IPCC, 1990. *Climate Change: The IPCC Scientific Assessment*. J.T. Houghton, G.J. Jenkins, and J.J. Ephraums, eds. Cambridge: Cambridge University Press.

IPCC, 1994. *Climate Change 1994: Radiative Forcing of Climate Change*. J.T. Houghton, L.G. Meira Filho, B.A. Callander, N. Harris, A. Kattenberg and K. Maskell, eds. Cambridge: Cambridge University Press.

IPCC, 1995. *Climate Change 1995, The Science of Climate Change.* J.T. Houghton, L.G. Meira Filho, B.A. Callander, N. Harris, A. Kattenberg and K. Maskell, eds. Cambridge: Cambridge University Press.

Kaye, J.A., S.A. Penkett, and F.M. Ormond, 1994. *Report on concentrations, lifetimes, and trends of CFCs, halons, and related species*. NASA Publication 1339. Washington: National Aeronautics and Space Administration.

Kerr, J.B., 1997. Observed dependences of atmospheric UV radiation and trends. Pages 259–265 in *Solar Ultraviolet Radiation Modelling, Measurements and Effects*. NATO ASI Series, Vol I 52. C. S Zerefos and A. F. Bais, eds. Berlin: Springer-Verlag.

Kerr, J.B., and C.T. McElroy, 1993. Evidence for large upward trends of ultraviolet-B radiation linked to ozone depletion. *Science*, **262**, 1032–1034.

Kerr J.B., and C.T. McElroy, 1994. Analyzing ultraviolet-B radiation: is there a trend? *Science,* **264**, 1342–1343.

Kerr J.B., C.T. McElroy, D.W. Tarasick, and D.I. Wardle, 1994. The Canadian Ozone Watch and UV-B advisory programs. Pages 794–797 in *Ozone in the troposphere and stratosphere.* Proceedings of the Quadrennial Ozone Symposium 1992, NASA Conference Publication 3266. Berlin: Springer-Verlag.

Komhyr, W.D., 1980. *Operations handbook – ozone observations with a Dobson spectrophotometer*, WMO Ozone Report No. 6. Geneva: World Meteorological Organization.

Krueger, A.J., L.S. Walter, P.K. Bhartia, C.C. Schnetzler, N.A. Krotkov, I. Sprod, and G.J.S. Bluth, 1995. Volcanic sulfur dioxide measurements from the total ozone mapping spectrometer instruments. *J. Geophys. Res.,* **100,** 14057–14076.

Lubin, D., and E.H. Jensen, 1995. Effects of clouds and stratospheric ozone depletion on ultraviolet radiation changes. *Nature,* **377,** 710–713.

Madronich S., 1992. Implications of recent total ozone measurements for biologically active ultraviolet radiation reaching the Earth's surface. *Geophys. Res. Lett.,* **19**, 37–40.

Mayer B., G. Seckmeyer, and A. Kyling, 1997. Systematic long-term comparison of spectral UV measurements and UVSPEC modeling results. *J. Geophys. Res.,* **102,** 8755–8767.

Puckrin E., W.F.J. Evans, and T.A.B. Adamson, 1996. Measurement of tropospheric ozone by thermal emission spectroscopy. *Atmos. Environ*., **30**, 563–568.

Quaite, R.E., B.M. Sutherland, and J.C. Sutherland, 1992. Action spectrum for DNA damage in alfalfa lowers predicted impact of ozone depletion. *Nature,* **358,** 576–578.

Ramanathan, V., L. Callis, R. Cess, J. Hansen, I. Isaksen, W. Kuhn, A. Lacis, F. Luther, J. Mahlman, R. Reck, and M. Schlesinger, 1987. Climate-chemical interactions and effects of changing atmospheric trace gases. *Rev. Geophys*., **25**, 1441–1487.

Schwander, H., P. Koepke, and A. Ruggaber, 1997. Uncertainties in modeled UV irradiances due to limited accuracy and availability of input data. *J. Geophys. Res.,* **102**, 9419–9429.

Simmonds, P.G., and R.G. Derwent, 1991. Measurements of ozone and other radiatively active gases at Mace Head, Ireland. *Atmos. Environ*. **25A**, 1795–1808.

Sinha, A., and R. Toumi, 1996. A Comparison of climate forcings due to chlorofluorocarbons and carbon monoxide. *Geophys. Res. Lett*., **23**, 65–68.

Stamnes, K., S-C. Tsay, and K. Jayaweera, 1988. Numerically stable algorithm for discrete-ordinate-method radiative transfer in multiple scattering and emitting layered media. *Appl. Opt.,* **27,** 2502–2509.

Stamnes K., J. Slusser, and M. Bowen, 1991. Derivation of total ozone abundance and cloud effects from spectral irradiance measurements. *Appl Opt.,* **30**, 4418–4426.

WMO, 1991. *Scientific Assessment of Stratospheric Ozone: 1991.* World Meteorological Organization Global Ozone Research and Monitoring Project, Report No. 25. Geneva: World Meteorological Organization.

WMO, 1994. *Scientific Assessment of Stratospheric Ozone: 1994*, World Meteorological Organization Global Ozone Research and Monitoring Project, Report No. 37. Geneva: World Meteorological Organization.

Zerefos C.S., A.F. Bais, C. Meleti, and I.C. Ziomas, 1995. A note on the recent increase of solar UV-B radiation over northern middle latitudes. *Geophys. Res. Lett*, **22**, 1245–1247.